PROCEEDINGS, 48th Workshop on Geothermal Reservoir Engineering
Stanford University, Stanford, California, February 2-6, 2022
SGP-TR-223

# Numerical Investigations of Tensile Induced Debonding Due To Temperature Variation in Geothermal Wells

Catalin TEODORIU[1], Ionut LAMBRESCU[2]

[1]The University of Oklahoma, USA, [2]Oil and Gas University of Ploiesti, Romania

cteodoriu@ou.edu

**Keywords:** well construction, geothermal, cement, debonding, shear versus tensile

## ABSTRACT

Geothermal wells experience higher loads compared with conventional oil and gas wells because of thermal cycles that inevitable exist during production and non-production phases. A conventional well construction utilizes and relies on cement for annular isolation between the casing and the formation; the isolation effectiveness depends on the cement behavior in downhole conditions after a given time. To date, only few alternatives to oil well cements have been economically imposed on the market. Geothermal wells are often exposed to temperature variations during their lifetime. In a previous study, we have shown that shear bonding strength is limited and decrease with curing temperature of the cement. In a newer study, we have investigated the tensile debonding of cement-casing system as a function of casing size and temperature variation. While most of the past studies focused mainly on debonding or not debonding situation, our detailed finite element study focused on the size of the debonding gap, the so-called micro annulus. We found that tensile debonding can occur at relatively low temperature variation and this failure will result in a micro annulus that will affect the geothermal well integrity. Furthermore, our study found that the surrounding formation properties could play a positive role towards casing-cement debonding.

## 1. INTRODUCTION

Currently, geothermal well construction follows the oil and gas well standards and configurations. It is, however, accepted that two major parameters significantly influence the decisional level: need of a larger flow area (hence larger production casing size and in many cases elimination of the tubing) and the presence of high temperature (in some cases higher than most of the high-pressure high temperature oil wells) (Teodoriu et al. 2022).

Although alternative solutions are currently in research phase (Teodoriu, 2021, 2022), Portland cement is still the preferred annular isolation and casing to formation sealing method for both oil and gas as well as for geothermal wells.

Well integrity and annular isolation play a key role in well performance and well completion in the oil, gas or geothermal industries. Cement is intended to provide hydraulic isolation, and prevent fluid flow between producing zones, protecting groundwater aquifers and surface sustained pressure (Loizzo and Sandeep, 2008, Al Ramis et al., 2020). However, the cement sheath alone is not always able to deliver an acceptable long-term solution for today's demanding drilling environment. Recently, advances in cement and well completion practices have significantly improved the quality of wells and extended their operating life. A possible future evolution of geothermal well construction is shown in Figure 1, whereas the option of a pure monobore well construction will allow geothermal well to be drilled in most complex geologies.

In an attempt to standardize these parameters, Teodoriu (2020) has introduced a new definition of the cement interfacial interactions and properties. Accordingly, the following cement properties are important for the interfacial cement – casing interactions:

- Shear Bonding Stress (Interfacial Bonding Shear Strength - IBSS) is an interfacial property that shows the force to shear the cement at the interface. (i.e. between casing and cement)
- Tensile Bonding Stress (Interfacial Bonding Tensile Strength - IBTS) is another interfacial cement property that shows the force to axially remove the cement from interface.
- Shear Stress (Pure Shear Strength - PSS) is a mechanical property like Unconfined Compressive Strength and Tensile Strength. The pure cement shear stresses occur because of the difference between the outer diameters of casings and couplings.
- Ultimate Unconfined Strength (UCS) is the cement resistance to compression and it is commonly used for reference purposes only.

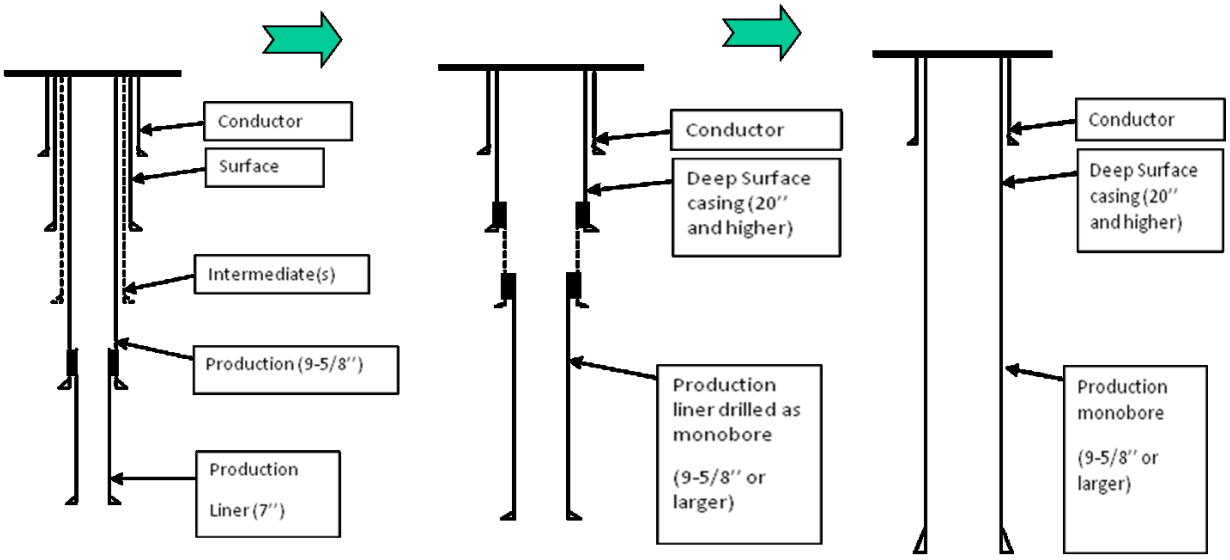


**Figure 1. Possible Evolution of Geothermal Well Construction**

## 2. FINITE ELEMENT MODELING OF CEMENT BONDING / DEBONDING

We used the 2021 R2 ANSYS version to perform the finite element simulation. The same axis symmetric model was used as presented in [10]. The model and its mesh are shown in Figure 2.

Figure 2.a presents the mesh, while Figure 2.b the boundary conditions. The pipe and cement are fixed for a length l (l is L/100, where L is the pipe and cement system length). We performed analyses for L=2000 mm, 10000 mm and 100000 mm. For some analyses, the cement exterior interaction with the rock (soil) was modeled with elastic support, while for other analyses, the cement exterior is considered free. Two major models have been considered for this study: The cement is free to move in radial direction (free boundary) and the cement outer boundary has limited radial movement (elastic boundary), meaning that the cement and rock are bonded through an elastic component. Both systems are free to move in axial direction, but the entire casing – cement system is fully restricted in all directions at the top of the model. As a note, we do not report any stress or strain in that zone, as that is not the focus of the simulation, but it is necessary in order to achieve the stability of the model. The free boundary model takes into account the non-existing or negligible cement-rock bonding scenario.

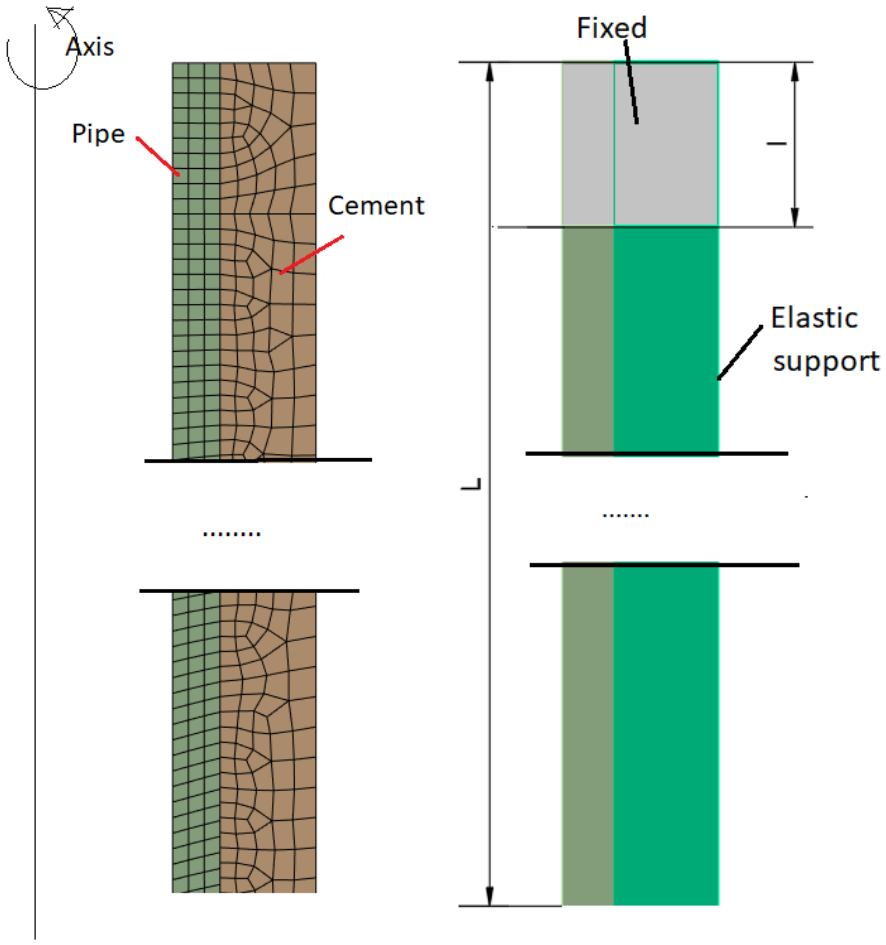


a. Mesh b. Boundary Conditions

**Figure 2. Model and Meshing Structure**

Table 1 presents the gap and axial displacements for a 2 m, 10 m and 100 m model, considering elastic support for the exterior cement diameter, free exterior diameter, and a mixed debonding mechanism. The gap is practically the same for all three cases (2, 10 and 100 m), and the axial displacement is linearly proportional () with the length of the pipe/cement. The table also shows scaled values (recorded values divided by the ratio between the pipes lengths) of the axial displacements. The differences are extremely low, with an error not exceeding 1%. Figures 3 and 4, respectively, present plots of the gaps for free cement or elastic supported cement, and axial displacements for the same three cases (2, 10 and 100 m).

**Table 1.** The effect of model length on the radial (Gap) and axial displacement

| CZM Models | Gap [mm] | | Axial Displacement [mm] | | Adjusted Values | |
|---|---|---|---|---|---|---|
| | Elastic boundary | Free Boundary | Elastic Boundary | Free Boundary | Elastic Boundary | Free Boundary |
| 2 m Model | 0.34398 | 0.11707 | 5.2918 | 4.7114 | 5.2918 | 4.7114 |
| 10 m Model | 0.34398 | 0.12276 | 26.445 | 23.254 | 5.289 | 4.6508 |
| 100 m Model | 0.34398 | 0.12304 | 267.11 | 253.91 | 5.3422 | 4.6782 |

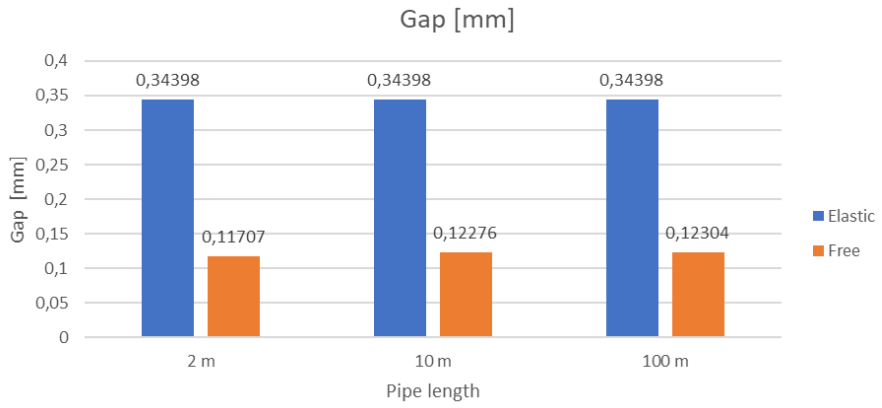


**Figure 3. Calculated Gap for 2, 10 and 100 m**

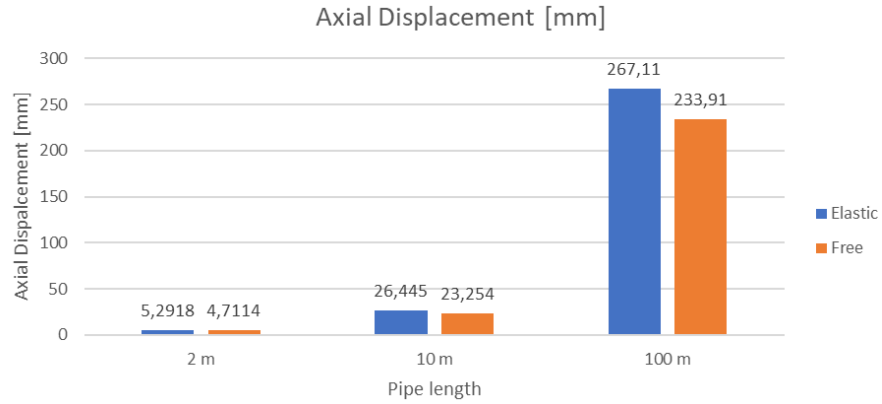


**Figure 4. Calculated Axial Displacement for 2, 10 and 100 m**

All the data above allows us to conclude that analyses for the 2 m pipe/cement length are representative for a long pipe/cement section. This significantly reduces the problem dimensions, with benefits in terms of computing time.

### 2.1. Model Formulation and Contact Zones

Quadratic axisymmetric elements with three or four edges were used for the whole cell in order to obtain better results. The contact between the cement and the external face of the pipe was modeled as bonded, followed by application of a CZM (Cohesive Zone Material). The bilinear model, Mode I, II and mixed debonding mechanisms were chosen for the CZM.

The parameters set in the Engineering Data section in Ansys Manual (Ansys, 2022) are:

- $T_{tmax}$—Maximum Equivalent Tangential Contact Debonding (the value of this parameter will be extracted from the experimental work);
- δt*—Tangential Slip at the Completion of Debonding (this value will also be extracted from the experimental data)

Artificial Damping Coefficient – according to Ansys Manual (Ansys, 2022), this parameter is used for convergence purposes only, and is normally related to the incremental time step used for the simulation.

### 2.2. Load Application and Boundary Definition

A Thermal Condition to simulate cooling of the cell with 100, 200 or 300 °C was the only load applied. Since the cement and the pipe have different ccoefficients of thermal expansion, debonding is expected to be favored at the interface between the two materials. The mechanical properties used for cement and steel are shown in Table 2.

**Table 2.** Mechanical properties for steel and cement materials used for the study

| Material | Young's Modulus (MPa) | Poisson Ratio (-) |
|---|---|---|
| Cement | 9,000 | 0.3 |
| Steel | 210,000 | 0.3 |

### 2.3. Failure Mode Definition

When the cell cools, differences in pipe and cement contraction tend to produce a gap between the two (thought as a Mode I debonding), but a Mode II debonding is also possible, since the pipe and the cement contract axially differently. Since there is no structural load applied (pressure or pushing force), we cannot speak about a failure mode in the traditional way. However we used the methodology proposed by Lambrescu et al. (2021) to estimate when the contact is broken, hence the unconventional failure mode used for this paper.

## 3. GEOTHERMAL WELL CEMENT MODELS AND RESULTS

We modeled the system with both CZM models active (mixt Mode), but we also ran simulations with single CZM mode (Type I for tensile or Type II for shear), although in practice it is hard to imagine that the two modes can be separated.

We considered 3 different temperature variations labeled as Delta T which represent the difference between the casing cement system initial temperature and the final temperature. Table 3 shows all cases studied for this paper. A total of 18 runs have been performed for modeling the cooling situation (temperature drops with 100, 200 and 300°C), and another 18 runs for the heating situation (temperature rises with 100, 200 and 300°C).

Since we stated that the 2m pipe/cement case produces results relevant for 10 and 100 m pipe/cement assembly, Table 4 shows the gap and the axial displacements for cases with Delta T 200°C, cooling/heating, elastic support/free cement. Values in brackets are for free boundary case.

**Table 3.** Scenarios used for this study.

| CZM Models | Mixt (Type I and II) | Type I | Type II |
|---|---|---|---|
| Elastic Boundary | Delta T (100, 200, 300 °C) | Delta T (100, 200, 300 °C) | Delta T (100, 200, 300 °C) |
| Free Boundary | Delta T (100, 200, 300 °C) | Delta T (100, 200, 300 °C) | Delta T (100, 200, 300 °C) |

**Table 4.** Gap and axial displacement for Delta T 200°C, 2 m pipe/cement assembly

| CZM Models | Type I | | Type II | | Mixt (Type I and II) | |
|---|---|---|---|---|---|---|
| | Cooling | Heating | Cooling | Heating | Cooling | Heating |
| Gap [mm] | 0.34398 (0.12279) | 0 (0) | 0.16476 (0.06867) | 0 (0) | 0.34398 (3.11707) | 0 (0) |
| Axial Displacement [mm] | -5.2918 (-4.6603) | 5.5923 (4.6599) | -5.5891 (-4.6562) | 5.6014 (4.6574) | -5.2918 (-4.7114) | 5.6017 (4.6577) |

Figure 5 shows the results of 6 simulations in which the boundary conditions have been changed from free-to-move outer cement layer (poor cement rock bonding) to elastic (deformable) rock system. We noticed that the elastic boundary scenario led to larger gap size when compared with free-to-move outer boundary. Figure 6 shows the axial displacement obtained for the same two outer boundaries conditions. Similar to the gap scenario, the simulation results for the mixt case and the Type I case are very close, while the Type II case leads to slightly different results. This will be discussed further in next part of the paper.

Figure 7 shows a comparison of all gaps for 3 different temperature levels: 100°C, 200°C and 300°C. The 100°C means that the casing cement system is exposed to a differential cooling of 100°C, for example from 120°C to 20°C. Such situations are common in geothermal wells when the well is cooled down for various reasons (logging, stimulation, workover). As expected, the gap magnitude increases with delta T increase. It should be noted that for Type II CZM model the simulation reached no convergence and thus could not solve the scenario. This can be explained by the fact that once shear debonding is achieved (Type II) the casing acts as independent from cement and thus the system loses its convergence.

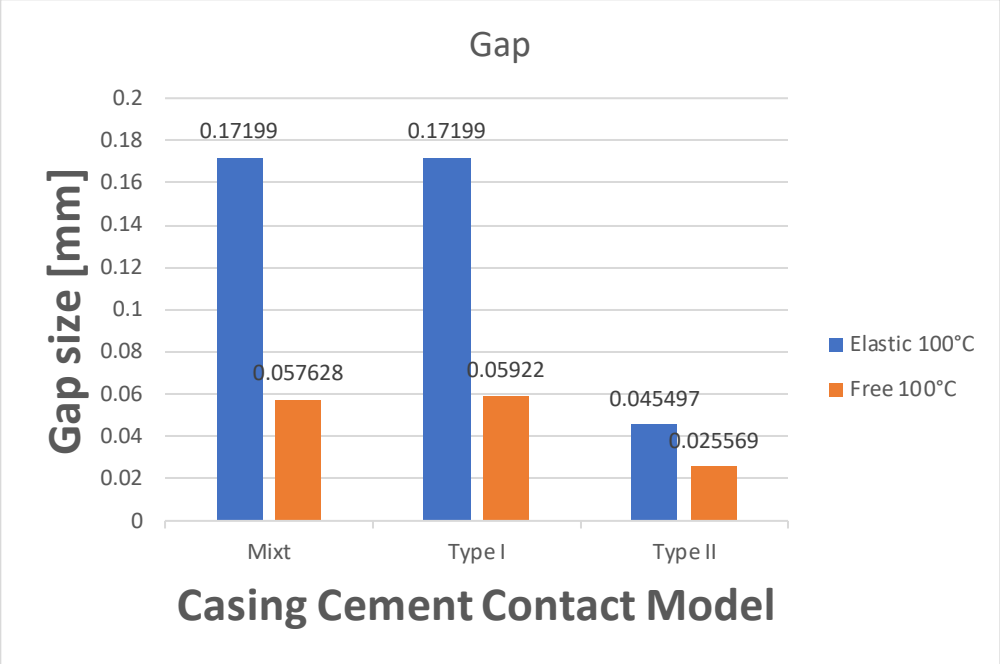


**Figure 5. Gap Size for 100°C Cooling Scenario**

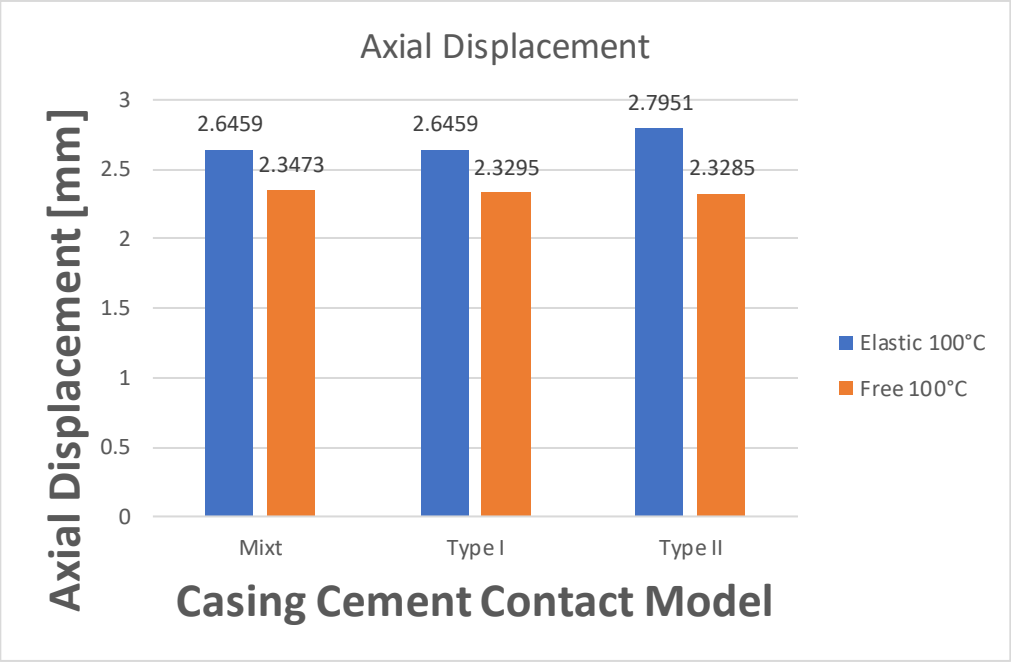


**Figure 6. Axial Displacement for 100°C Cooling Scenario**

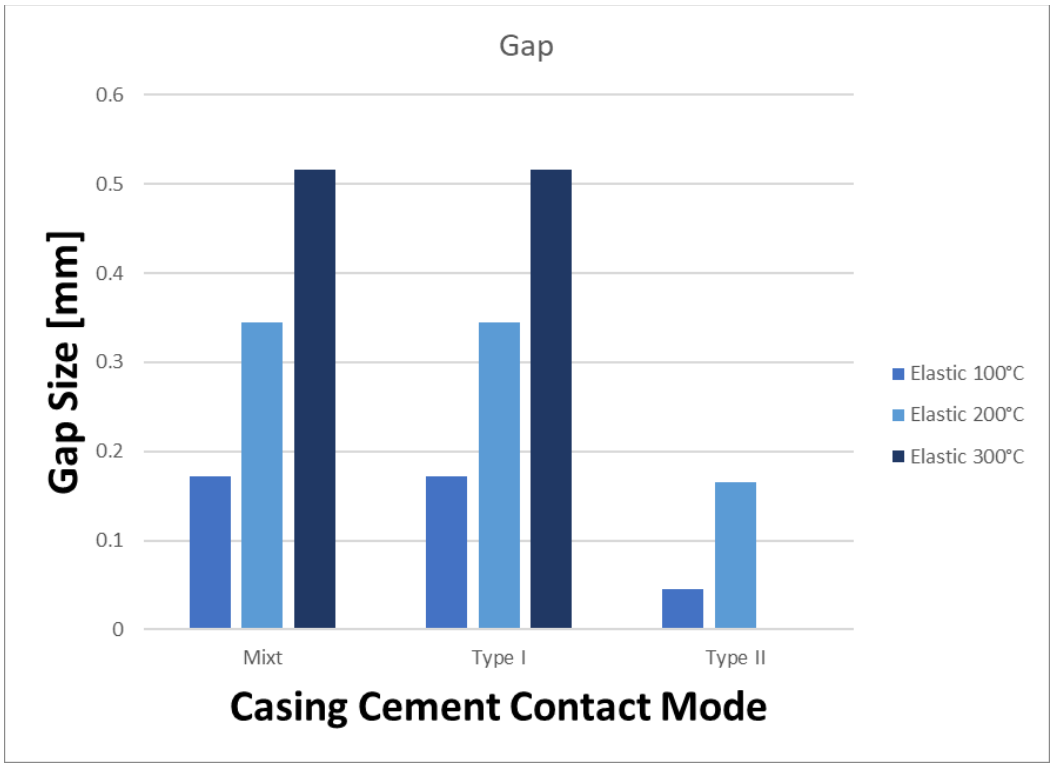


**Figure 7. Effect of Temperature Change Amplitude on Gap Size.**

Figure 8 shows the model deformation at 200°C differential cooling, capturing the radial (gap) and axial displacement for the two main scenarios used in this paper: free boundary and elastic boundary. As already shown in Figure 7, the whole system deformation clearly shows that the elastic boundary leads to a much larger radial gap (debonding) because the cement rock bond does not allow the cement to move freely when the casing shrinks. Figure 9 shows the system deformation for the heating scenario. Radial debonding is not present during the heating scenario since the casing pushes towards the cement.

We noticed that the free boundary case leads to less axial cement shrinkage when compared with elastic boundary case. This can be explained by the fact that the free boundary case allows the cement to change its dimensions in all directions while limited bonding with the rock as in the case of elastic boundary leads to limited cement shrinkage. The existence of a different elongation of the cement and casing also leads to the conclusion that shear between cement and casing will be induced at one moment.

A comparison of the axial and radial displacement for debonding modes during cooling leads to a very interesting observation shown in Figure 10. While Mode I shows a clear uniform forming gap along the entire interfacial casing-cement contact, Mode II shows debonding failure only at the free end of the model (lower end in Figure 10). This observation is very important when we compare with the mixt mode scenario, which shows clearly that tensile cement debonding is the main driver during the cooling process, which is the least documented in literature. Our models show that also in case of Type II CZM model a radial debonding over a short length takes place at the bottom of the model. The debonding length seems to be a function of the temperature difference but does not propagate through the entire length of the model like the Type I scenario where it is clear to see that a total debonding takes place between casing and cement.

To better highlight when debonding takes place and which mode is primary failure mode, we have extracted the equivalent differential temperature at which a failure gap is generated. Table 5 shows the calculated values at when a debonding will appear, which is based on the methodology presented by Lambrescu (Lambrescu and Teodoriu, 2022, Lambrescu et al., 2021) to detect the debonding initiation point. It can be seen that it requires only 60°C of cooling to reach a type I (tensile) debonding and 174°C for Type II (shear) debonding.

**Table 5.** Temperature difference at which failure occurs.

| CZM Models | Mixt (Type I and II) | Type I | Type II |
|---|---|---|---|
| Elastic Boundary | Delta T 60°C | Delta T 60°C | Delta T 174°C |

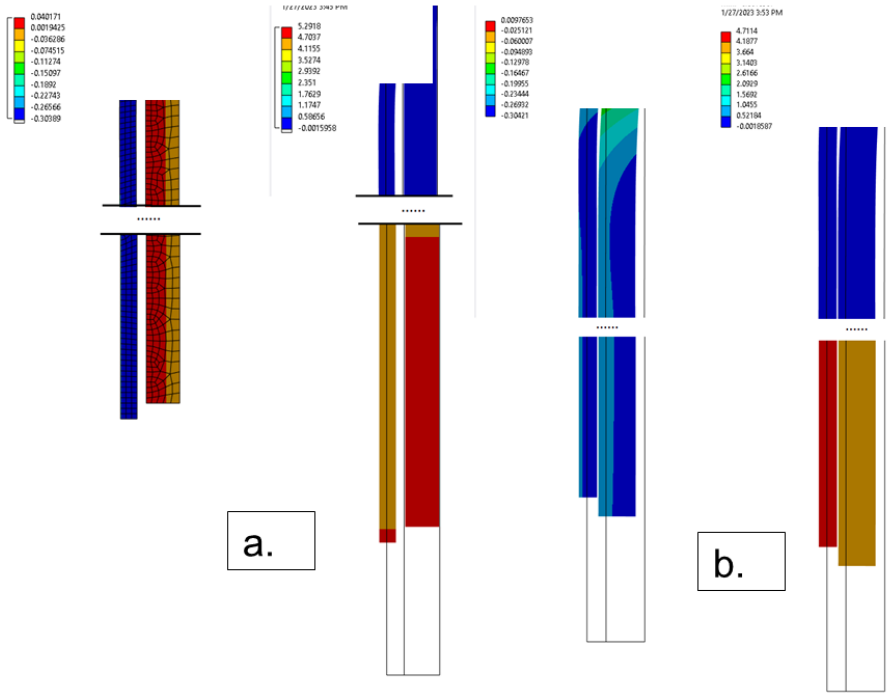


**Figure 8. System Deformation Comparison for 200°C Differential Cooling**

a. Delta t 200°C. Radial and Axial Displacement. Cooling, Elastic Boundary, Mixed Mode

b. Delta t 200°C. Radial and Axial Displacement. Cooling, Free Boundary, Mixed Mode

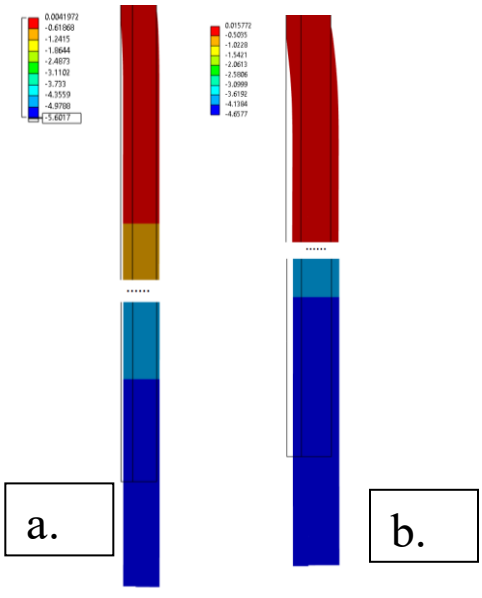


**Figure 9. System Deformation Comparison for 200°C Differential Heating**

a. Delta t 200°C . Axial Displacement. Heating, Elastic Support, Mixed Mode

b. Delta t 200°C. Axial Displacement. Heating, Free Cement, Mixed Mode

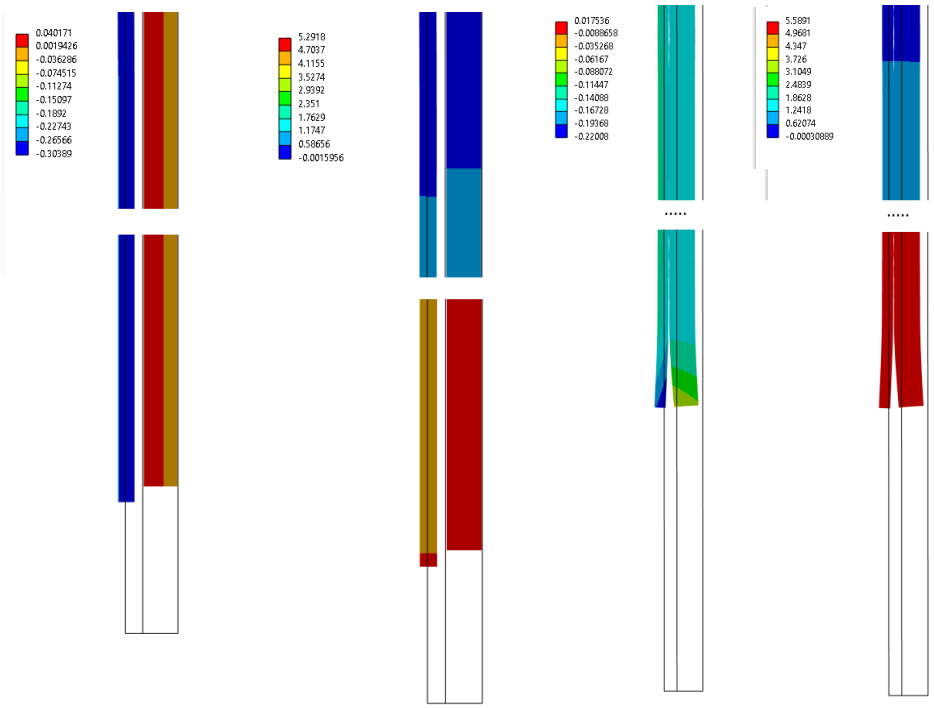


**Figure 10. System Radial and Axial Deformation Comparison for 200°C Differential Cooling for Type I (left) and II CZM bonding (right).**

## 4. CONCLUSIONS

An intensive finite element study has been performed to understand the main debonding criteria of casing cement system in geothermal wells.

Cooling and heating situations have been modeled for three CZM modes: Type I (tensile), Type II (shear) and mixt (Type I and II simultaneously).

We found out that Type I failure mode is the most important in cooling scenarios, and the casing cement will first debond in radial direction.

Although not conclusive at this stage, it seems that Type II debonding appears during heating. Currently, this scenario is still under research in order to include friction and other factors into the simulation.

## REFERENCES

Al Ramis, H., Teodoriu, C., Bello, O., Al Marhoon, Z, 2020. High-Definition Optical Method for Evaluation of Casing-Cement Microannulus (CCMA). J Petrol Sci Eng. 2020; 195:107719. https://doi.org/10.1016/j.petrol.2020.107719.

Loizzo, M., Sandeep, S., 2008. Assessing Long-term CO2 Containment Performance: Cement Evaluation in Otway CRC-1. Paper presented at the SPE Asia Pacific Oil and Gas Conference and Exhibition, Perth, Australia, October 2008. doi: https://doi.org/10.2118/115707-MS" https://doi.org/10.2118/115707-MS.

Lambrescu, I., Teodoriu, C., 2022, Experimental and Numerical Investigations of Cement Bonding Properties at Elevated Temperatures—The Effect of Sample Cooling, Materials, V 15, N 14, P 4955, 1996-1944, MDPI

Lambrescu, I., Teodoriu, C., Amani, M., 2021, Experimental and Numerical Investigations of Cement Bonding Properties. Materials 2021, 14, 7235.https://doi.org/10.3390/ ma14237235

Teodoriu, C., Esquitin, Y., Vasques, R., 2022, Can Geothermal Wells Go Cementless?, 2022 Stanford Geothermal Workshop

Teodoriu, C., Bello, O., Vasquez, R. R., Melander, R. M., and Esquitin.Y. 2021, "Cementless Well Construction Opens the Full Control on Well Integrity for the Life of the Well." Paper presented at the SPE Annual Technical Conference and Exhibition, Dubai, UAE, September 2021. doi: https://doi.org/10.2118/206052-MS